

Novel Carbazole-Phenothiazine Dyads for Dye-Sensitized Solar Cells: A Combined Experimental and Theoretical Study

Gabriele Marotta,[†] Marri Anil Reddy,[‡] Surya Prakash Singh,[‡] Ashraful Islam,[§] Liyuan Han,[§] Filippo De Angelis,^{*,†} Mariachiara Pastore,^{*,†} and Malapaka Chandrasekharam^{*,‡}

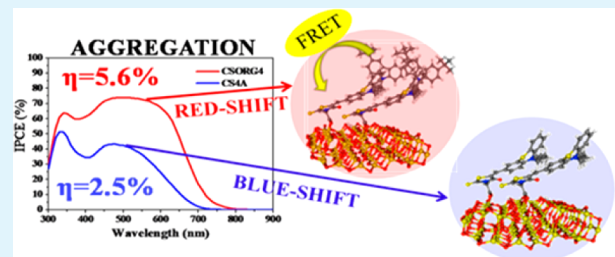
[†]Computational Laboratory for Hybrid Organic Photovoltaics (CLHYO), Istituto CNR di Scienze e Tecnologie Molecolari, via Elce di Sotto 8, I-06123, Perugia, Italy

[‡]Network of Institutes for Solar Energy (CSIR-NISE), Inorganic & Physical Chemistry Division, CSIR—Indian Institute of Chemical Technology, Uppal Road, Tarnaka, Hyderabad -500607, India

[§]Photovoltaic Materials Unit, National Institute for Materials Science, 1-2-1 Sengen, Tsukuba, Ibaraki 305-0047, Japan

ABSTRACT: We report a joint experimental and computational work on new organic donor–acceptor dye sensitizers in which a carbazole (CZ) and a phenothiazine (PTZ) units are linked together by an alkyl C₆H₁₃, while two different anchoring groups are employed: the cyanoacrylic acid (CS1A, CSORG1) and the rhodanine-3-acetic acid (CS4A, CSORG4). The CZ moiety has multiple roles of (i) acting as an extra-electron donor portion, providing more electron density on the PTZ; (ii) suppressing the back-electron transfer from TiO₂ to the electrolyte by forming a compact insulating dye layer; (iii) modulating dye aggregation on the semiconductor surface; and (iv) acting as an antenna, collecting photons and, through long-range energy transfer, redirecting the captured energy to the dye sensitizer. We show that the introduction of the CZ donor remarkably enhances the photovoltaic performances of the rhodanine-based dye, compared to the corresponding simple PTZ dye, with more than a two-fold increase in the overall efficiencies, while it does not bring beneficial effects in the case of the cyanoacrylic-based sensitizer. Based on quantum mechanical calculations and experimental measurements, we show that, in addition to a favored long-range energy transfer, which increases the light absorption in the blue region of the spectrum, the presence of the CZ unit in the CSORG4 dye effectively induces a beneficial aggregation pattern on the semiconductor surface, yielding a broadened and red-shifted light absorption, accounting for the two-fold increase in the generated photocurrent.

KEYWORDS: DSSC, organic dyes, phenothiazine, carbazole, FRET, aggregation, DFT



1. INTRODUCTION

Dye-sensitized solar cells (DSSC)^{1–3} offer a promising alternative to conventional silicon-based solar technologies, providing high efficiency, reduced fabrication costs, and short energy payback time. In these cells, the dyes and the mesoporous TiO₂ layer⁴ represent the key components to achieve high power conversion efficiencies. Although the highest-performance devices employing a liquid I⁻/I₃⁻ electrolyte⁵ are sensitized with Ru(II)-based dyes such N3, N719, and black dye,^{4,6–8} several promising metal-free dyes are developed,^{9,10} with overall efficiencies approaching 10%.^{11,12} In comparison to Ru(II)-based dyes, organic dyes exhibit many advantages, such as ease of molecular structures design and synthesis, high molar extinction coefficients, the possibility of extending absorption spectra in the visible range as a result of incorporation of different light-absorbing groups, and reduced production costs. A typical push–pull organic dye consists of an electron-donating group, a linker group, and an electron accepting/anchoring group. Among the donor moieties, *N,N*-dimethylaniline group,^{13,14} coumarins,^{15–21} tetrahydroquinolines,^{22,23} pyrrolidine,²⁴ carbazoles,²⁵ diphenylamine,²⁶ triphe-

nalamine,^{27–30} etc. have been widely employed. On the other side, basically three types of acceptor/anchor groups—namely, cyanoacrylic acid,^{13–31} carboxylic acid,^{32–34} and rhodanine-3-acetic acid^{35–37}—are widely used in organic dyes for DSSC.^{11,12} Moreover, in conjunction with novel ferrocene or cobalt-based electrolytes, organic dyes achieved better performance, compared to Ru(II) dyes.^{38–42} The reduced efficiencies (lower open-circuit voltage (V_{oc}) values)⁴³ of organic sensitizers with standard the I⁻/I₃⁻ redox mediator have been commonly attributed to higher charge recombination of the injected electrons with the oxidized dye or electrolyte; also, the formation of dye-aggregates on the TiO₂ surface has been recognized as one of the factors yielding lower photovoltaic performance of DSSCs based on organic dyes.^{44–52} While dye aggregation can be successfully prevented by the use of anti-aggregation co-adsorbents,^{53–58} the effect of the dye molecular structure on the recombination kinetics is more entangled and

Received: July 5, 2013

Accepted: September 11, 2013

Published: September 11, 2013



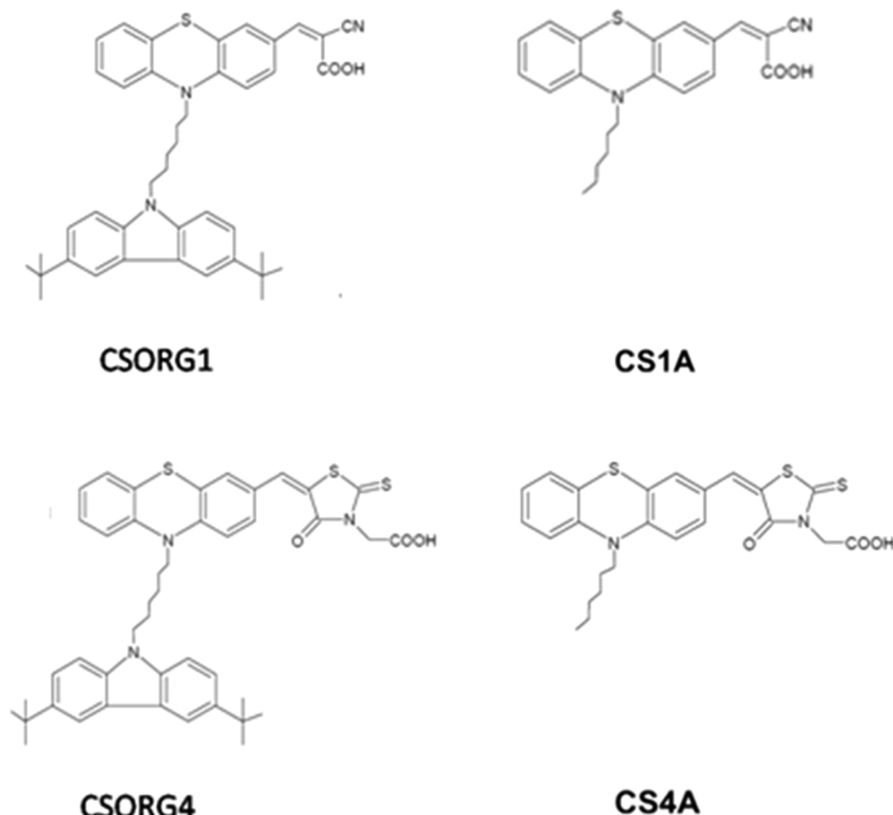


Figure 1. Molecular structure of the CSORG1, CSORG4, CS1A, and CS4A sensitizers.

has been investigated for both metal-based^{59–62} and metal-free dyes.^{46,51,63–68} In this context, elucidating the subtle relations existing between the dye molecular structure and the final photovoltaic performances is a fundamental requisite for a successful strategic molecular design of novel sensitizers.

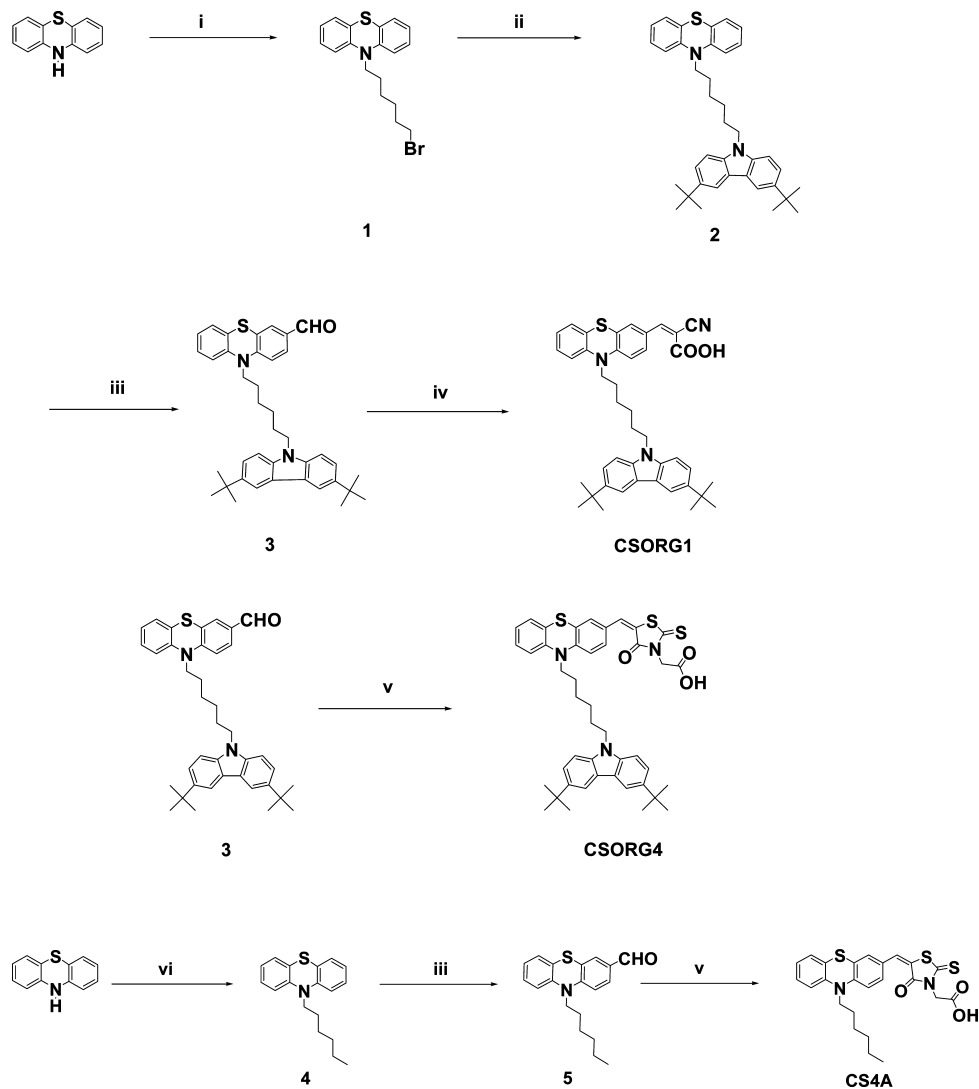
From a different perspective, an appealing molecular engineering strategy to enhance the dye efficiency by extending the window of absorbed light consists of the use of “antenna” systems, tethered to the dye, which collect photons and, through long-range energy transfer (Förster resonance energy transfer, FRET),⁶⁹ divert the captured energy to the sensitizing dye, grafted to the TiO₂ surface.⁷⁰ With respect to various co-sensitization strategies, where different dyes are adsorbed on the semiconductor surface,^{71,72} the benefit of linking the antenna to the dye lies in the possibility of combining multiple absorbing dyes, overcoming the restrictions of the limited TiO₂ loading as well as those involved in the effective tuning of the inter-chromophoric distance/geometry to increase the FRET efficiency.^{73–75} We recall that FRET is an excitation transfer mechanism mediated by the coupling of two resonant dipoles in the presence of an electric field.⁷⁶ Therefore, the geometry of the donor–acceptor system is crucial to determining the Förster radius (R_0) and, hence, the energy transfer rate.⁷³ The Förster radius, defined as the distance between the donor and the acceptor when the FRET has 50% probability,⁷⁶ is, indeed, given by the energy donor photoluminescence quantum efficiency (Q_D), the overlap integral of the donor emission spectrum (F_D), and the acceptor absorption spectrum (ϵ_A), and the orientation factor (κ^2), given by the relative orientation of the two interacting dipole moments.⁷⁷

Theoretical and computational modeling of stand-alone dyes and of dye-sensitized TiO₂ heterointerfaces^{47,64,78} represents a

powerful tool toward understanding the factors leading to enhanced photovoltaic efficiency. Here, we report a joint experimental and computational work on new organic donor–acceptor dye sensitizers in which a carbazole (CZ), possibly acting as an antenna, and a phenothiazine (PTZ) unit, anchored to the TiO₂, are linked by an alkyl C₆H₁₃, employing two different anchoring groups: the cyanoacrylic acid (CS1A, CSORG1) and rhodanine-3-acetic acid (CS4A, CSORG4). We compare the photovoltaic performances of the new CSORG1 and CSORG4 dyes with those of the corresponding (CZ-free) PTZ-derivative, CS1A⁷⁹ and CS4A⁸⁰ (see Figure 1).

Several examples of phenothiazine-based dyes have been reported in the literature,^{79–92} with generally high V_{oc} values and good overall efficiencies. On the other side, the use of the CZ ring in organic^{66,67,93–95} and ruthenium-based^{96–98} dyes is well-documented.^{73,99,100} To the best of our knowledge, however, this is the first example of pure metal-free dyads for DSSC applications. Here, we introduce the CZ moiety linked via a C₆H₁₂ alkyl chain with the multiple objectives of (i) acting as an extra-electron donor portion, providing more electron density on the PTZ; (ii) suppressing the back electron transfer from TiO₂ to electrolyte by forming a compact insulating dye layer; (iii) modulating dye aggregation on the semiconductor surface; and (iv) assessing the possibility of exploiting FRET⁶⁹ to produce additional photocurrent. Our results reveal a negligible effect of the CZ unit when linked to the CS1A dye (CSORG1, Figure 1), while a marked improvement of the photovoltaic performances in the rhodanine-based CS4A dye (CSORG4, Figure 1) is obtained, with a sizeable extension of the light to current conversion efficiency up to 800 nm and a twofold increment in the generated photocurrent. We show that the different anchoring groups in CSORG1 and CSORG4

Scheme 1



give rise to different adsorption geometries on the oxide surface and to a different tendency to form dye aggregates. This consequently induces a different geometrical arrangement of the CZ (antenna) and PTZ (sensitizing dye) units, resulting in a largely favored energy transfer in the rhodanine-based CSORG4 dye, which possibly contributes to enhancing increasing the current response in the 300–400 nm range. Moreover, the increased V_{oc} value observed for the CZ-PTZ CSORG4 dye suggests a possible blocking effect of the CZ unit, able to prevent electron recombination of the injected electrons with the electrolyte.

2. EXPERIMENTAL DETAILS

2.1. General Synthetic Procedure. The synthetic route of CSORG1, CSORG4, CS1A, and CS4A is shown in Scheme 1. Well-known organic reactions were used for the synthesis of these dyes, such as N-alkylation followed by Vilsmeier-Haack formylation. Then, the formylated product was subjected to Knoevenagel condensation with cyanoacetic acid and rhodanine-3-acetic acid. The detailed synthetic procedures for CSORG1, CSORG4, and CS4A dyes are described below.

2.2. Experimental Section. The starting materials phenothiazine, carbazole, dibromohexane, bromohexane, rhodanineacetic acid, and cyanoacetic acid were purchased from Sigma-Aldrich. The solvents

were purified by standard procedures and purged with nitrogen before use. All other chemicals used in this work were analytical grade and were used without further purification, and all reactions were performed under argon atmosphere. Chromatographic separations were carried out on silica gel (60–120 mesh). ^1H NMR and ^{13}C NMR spectra were recorded on an Avance 300 spectrometer and a 500 MHz spectrometer, using tetramethylsilane (TMS) as an internal standard. Mass spectra were recorded on a Shimadzu Model LCMS- 2010EV system that was equipped with an electrospray ionization (ESI) probe. Absorption spectra were recorded on a Shimadzu ultraviolet-visible light (UV-vis) spectrometer. Emission spectra were recorded on a Jobin Yvon Horiba Model Fluorolog 3 fluorescence spectrometer.

Reagents and Conditions. (i) NaH, dimethylformamide (DMF), and 1,6-dibromohexane, at room temperature (RT), refluxed overnight; (ii) potassium hydroxide (KOH), DMF, di-*tert*-butylcarbazole, at RT, for 6 h; (iii) DMF, POCl_3 , 1,2-dichloroethane, refluxed overnight; (iv) piperidine, CHCl_3 , cyanoacetic acid, refluxed for 8 h; (v) Rhodanine-3-acetic acid, ammonium acetate, acetic acid, refluxed for 3 h; and (vi) NaH, DMF, 1-bromohexane, at RT, refluxed overnight.

Synthetic Procedure for CSORG1 and CSORG4 Dyes. **10-(6-Bromohexyl)-10H-phenothiazine (1).** A 100-mL three-necked flask was charged with phenothiazine (2.00 g, 10.036 mmol), NaH (0.29 g, 12.043 mmol), and 30 mL of DMF. The resulting mixture was stirred for 30 min. 1,6-Dibromohexane (1.852 mL, 12.043 mmol) was then added and the mixture was stirred overnight at room temperature. The

reaction mixture was quenched with ice water (400 mL) and extracted three times with ethylacetate. The combined organic fractions were washed with brine and dried over Na_2SO_4 . The solvent was removed under reduced pressure and the residue was purified by silica gel column chromatography using *n*-hexane/ethylacetate (9/1; v/v) as the eluent to give viscous liquid **1** (82%). ^1H NMR (300 MHz, CDCl_3 , δ): 7.10–7.07 (t, 4H), 6.78–6.80 (d, 2H), 6.84–6.87 (d, 2H), 3.85 (t, 2H, N–CH₂), 3.31 (t, 2H, Br–CH₂), 1.83–1.79 (m, 4H), 1.46–1.43 (m, 4H). ^{13}C NMR (300 MHz, CDCl_3 , δ): 145.12, 127.35, 127.10, 124.99, 122.33, 115.37, 47.00, 33.71, 32.52, 27.63, 26.55, 25.92. ESI-MS for $\text{C}_{18}\text{H}_{20}\text{BrNS}$: Calcd 362.33, Found 364.

10-(6-(3,6-Di-tert-butyl-9H-carbazol-9-yl)hexyl-10H-phenothiazine (2). A suspension of powdered KOH (151 mg, 2.687 mmol) and dry DMF (10 mL) was stirred and degassed at room temperature for 60 min, and carbazole (300 mg, 1.075 mmol) and 10-(6-bromohexyl)-10H-phenothiazine (**1**) (427 mg, 1.183 mmol) were added. Then the reaction mixture was stirred for 6 h at room temperature and finally poured into ice water (200 mL). The organic layer was collected and the aqueous layer was extracted three times with ethyl acetate. The combined organic layers were dried over Na_2SO_4 , and the solvent was removed under reduced pressure, and the resulting crude oily was purified by silica gel column chromatography using petroleum ether/ethyl acetate (9:1) as eluent to give **2** (82%). ^1H NMR (300 MHz, CDCl_3 , δ): 8.01 (s, 2H), 7.37–7.41 (m, 2H), 7.14–7.25 (m, 4H), 7.06–7.09 (m, 3H), 6.74–6.88 (m, 3H), 4.18 (t, 2H, N–CH₂), 3.72–3.85 (b, 2H, N–CH₂), 1.72–1.86 (m, 4H), 1.44 (s, 18H), 0.83–0.9 (m, 4H). ^{13}C NMR (300 MHz, CDCl_3 , δ): 145.2, 141.34, 138.88, 127.41, 127.13, 124.97, 123.17, 122.56, 122.31, 116.17, 115.34, 107.94, 47.09, 42.82, 34.60, 32.04, 29.02, 26.88, 26.68. ESI-MS for $\text{C}_{38}\text{H}_{44}\text{N}_2\text{S}$: Calcd 560.83, Found 561.

10-(6-(3,6-Di-tert-butyl-9H-carbazol-9-yl)hexyl-10H-phenothiazine-3-carbaldehyde (3). To a solution of 10-(6-(3,6-di-tert-butyl-9H-carbazol-9-yl)hexyl-10H-phenothiazine (**2**) (800 mg, 1.426 mmol) and dry DMF (120 mg, 1.568 mmol) in 1,2-dichloroethane (DCE) (10 mL), POCl_3 (239 mg, 1.568 mmol) was added slowly at 0 °C in an ice water bath. Then, the mixture was heated at reflux and maintained overnight. The reaction mixture was quenched with water and extracted three times with chloroform. The combined organic fraction were washed with brine and dried over Na_2SO_4 . The solvent was removed under reduced pressure and the residue was purified by silica gel column chromatography using petroleum ether/ethylacetate (9/1; v/v) as an eluent to give **3** (75%). ^1H NMR (300 MHz, CDCl_3 , δ): 9.75 (s, 1H), 8.01 (s, 2H), 7.53–7.56 (m, 2H), 7.40 (d, 2H), 7.17 (d, 2H), 7.06 (d, 2H), 6.91 (t, 1H), 6.76 (t, 2H), 4.2 (t, 2H, N–CH₂), 3.8 (t, 2H, N–CH₂), 1.70–1.88 (m, 4H), 1.44 (s, 18H), 1.25 (broad, 4H). ^{13}C NMR (300 MHz, CDCl_3 , δ): 189.91, 150.58, 143.24, 141.38, 138.82, 130.94, 129.97, 128.29, 127.47, 125.00, 123.78, 123.49, 123.14, 122.53, 116.15, 115.86, 114.68, 107.87, 47.59, 42.76, 34.56, 31.96, 28.97, 26.75, 26.50, 26.41. ESI-MS for $\text{C}_{39}\text{H}_{44}\text{N}_2\text{OS}$: Calcd 588.84, Found 589.

CSORG1. Compound **3** (120 mg, 0.203 mmol) in CHCl_3 (8 mL) was condensed with 2-cyanoacetic acid (43 mg, 0.509 mmol) in the presence of piperidine (0.066 mL, 0.672 mmol). The mixture was refluxed for 8 h. After cooling to room temperature, 5 mL of 2 M aqueous HCl was added and the mixture was stirred for 30 min. Then the mixture was washed with water and extracted three times with chloroform. The combined organic fractions were washed with brine and dried over Na_2SO_4 . The solvent was removed under reduced pressure and the residue was purified by column chromatography using methanol/dichloromethane (1/9; v/v) as an eluent to afford **CSORG1** (75%) as dark red powder. ^1H NMR (300 MHz, CDCl_3 , δ): 8.01–8.03 (d, 3H), 7.89–7.92 (d, 2H), 7.58 (s, 2H), 7.39–7.42 (d, 2H), 7.16–7.19 (d, 2H), 7.03–7.09 (m, 2H), 6.89–6.94 (m, 1H), 6.72–6.80 (t, 2H), 4.2 (t, 2H, N–CH₂), 3.78 (t, 2H, N–CH₂), 1.71–1.89 (m, 4H), 1.44 (s, 18H), 1.25 (broad, 4H). ^{13}C NMR (300 MHz, CDCl_3 , δ): 149.11, 142.83, 141.41, 138.87, 131.44, 129.71, 127.41, 125.80, 124.37, 123.44, 123.39, 123.19, 122.59, 116.17, 115.61, 114.76, 107.95, 47.62, 42.82, 34.59, 32.03, 29.03, 26.84, 26.57, 26.40. FT-IR(KBr), cm^{-1} : 2218 (CN), 1710 (C=O), 1589, 1569, 1491, 1405,

1363, 1296, 1254, 1205, 1169, 878, 806, 751. ESI-MS for $\text{C}_{42}\text{H}_{45}\text{N}_3\text{O}_2\text{S}$: Calcd 655.89, Found 656.

CSORG4. To 15 mL of glacial acetic acid were added **3** (135 mg, 0.23 mmol) and rhodanine-3-acetic acid (48 mg, 0.252 mmol), and the solution was refluxed for 3 h in the presence of ammonium acetate (21 mg, 0.274 mmol). After cooling to room temperature, the mixture was poured into ice water. The precipitate was filtered and washed with distilled water. After drying under vacuum, the precipitate was purified by column chromatography using methanol/dichloromethane (1/9; v/v) as an eluent to afford **CSORG4** (80%) as red crystals. ^1H NMR (300 MHz, CDCl_3 , δ): 8.00 (s, 2H), 7.49–7.55 (broad, 1H), 7.38 (d, 2H), 7.13–7.18 (m, 4H), 6.99–7.03 (m, 2H), 6.83–6.90 (m, 1H), 6.66–6.69 (m, 2H), 4.78–4.87 (broad s, 2H, –CH₂COOH), 4.12–4.19 (broad s, 2H, N–CH₂), 3.66–3.74 (broad s, 2H), 1.63–1.87 (m, 4H), 1.42 (s, 18H), 1.25 (broad s, 4H). ^{13}C NMR (300 MHz, CDCl_3 , δ): 192.349, 172.21, 167.20, 143.18, 141.43, 138.86, 133.16, 131.03, 129.18, 127.48, 127.21, 123.35, 123.19, 122.58, 119.30, 116.21, 115.64, 115.20, 107.93, 47.57, 42.84, 34.60, 32.04, 29.06, 26.88, 26.61, 26.47. FT-IR(KBr), cm^{-1} : 1713 (C=O), 1587, 1568, 1491, 1464, 1402, 1326, 1299, 1251, 1195, 1110, 1055, 958, 908, 878, 805, 755, 666, 650, 612. ESI-MS for $\text{C}_{44}\text{H}_{47}\text{N}_3\text{O}_3\text{S}_3$: Calcd 762.06, Found 763.

Synthesis of CS4A. **10-Hexyl-10H-phenothiazine (4).** A 100-mL three-necked flask was charged with phenothiazine (2.00 g, 10.036 mmol), NaH (0.29 g, 12.043 mmol), and 30 mL of DMF. The resulting mixture was stirred for 30 min, and then bromohexane (1.806 mL, 12.043 mmol) was added and the mixture was stirred overnight at room temperature. The reaction mixture was quenched with ice water (400 mL) and extracted three times with ethyl acetate. The combined organic fractions were washed with brine and dried over Na_2SO_4 . The solvent was removed under reduced pressure and the residue was purified by silica gel column chromatography using *n*-hexane/ethyl acetate (9/1; v/v) as the eluent to give viscous liquid **4** (82%). ^1H NMR (300 MHz, CDCl_3 , δ): 7.05–7.10 (m, 4H), 6.78–6.87 (m, 4H), 3.81 (t, 2H), 1.74–1.83 (m, 2H), 1.25–1.44 (m, 6H), 0.86 (t, 3H). ^{13}C NMR (300 MHz, CDCl_3 , δ): 145.27, 127.34, 127.09, 124.84, 122.23, 115.32, 47.38, 31.43, 26.85, 26.62, 22.55, 13.95. ESI-MS for $\text{C}_{18}\text{H}_{22}\text{NS}$: Calcd 284.14675, Found 284.14709.

10-Hexyl-10H-phenothiazine-3-carbaldehyde (5). To a solution of 10-hexyl-10H-phenothiazine (**4**) (0.800 g, 2.836 mmol) and dry DMF (0.240 mL, 3.120 mmol) in 1,2-dichloroethane (DCE) (10 mL), POCl_3 (0.294 mL, 3.120 mmol) was added slowly at 0 °C in an ice water bath. The mixture then was heated at reflux and maintained overnight. The reaction mixture was quenched with water and extracted three times with chloroform. The combined organic fractions were washed with brine and dried over Na_2SO_4 . The solvent was removed under reduced pressure and the residue was purified by silica gel column chromatography using petroleum ether/ethyl acetate (8/2; v/v) as an eluent to give **5** (75%) as an yellow powder. ^1H NMR (300 MHz, CDCl_3 , δ): 9.78 (s, 1H), 7.63 (d, 1H), 7.57 (s, 1H), 7.58 (t, 1H), 7.105 (d, 1H), 6.86–6.97 (m, 3H), 3.88 (t, 2H), 1.77–1.84 (m, 2H), 1.25–1.47 (m, 6H), 0.87 (t, 3H). ^{13}C NMR (300 MHz, CDCl_3 , δ): 189.96, 150.65, 143.33, 130.92, 130.02, 128.28, 127.47, 124.89, 123.67, 123.48, 115.86, 114.69, 47.93, 31.31, 26.64, 26.44, 22.50, 13.92. ESI-MS for $\text{C}_{19}\text{H}_{21}\text{BrNOS}$: Calcd 312.14142, Found 312.14142.

CS4A. The product was synthesized according to the procedure as described above for the synthesis of **CSORG4**, starting from compound **5**, giving a dark red powder **CS4A** (85%). ^1H NMR (300 MHz, CDCl_3 , δ): 7.634 (s, 1H), 7.261–7.301 (m, 1H), 7.098–7.203 (m, 3H), 6.957 (t, 1H), 6.87 (d, 2H), 4.915 (s, 2H), 3.863 (t, 2H), 1.810 (q, 2H), 1.294–1.462 (m, 6H), 0.878 (t, 3H). ^{13}C NMR (300 MHz, CDCl_3 , δ): 192.395, 167.560, 166.891, 147.376, 142.966, 132.585, 130.478, 128.635, 127.103, 126.875, 126.739, 124.967, 122.890, 118.872, 115.432, 114.964, 44.182, 30.826, 26.170, 25.864, 21.971, 13.099. ESI-MS for $\text{C}_{24}\text{H}_{24}\text{N}_2\text{O}_3\text{S}_3$: Calcd 484.65, Found (M + 1)⁺ 485.07.

2.3. Device Fabrication. **2.3.1. Preparation of TiO₂ Electrode.** Nanocrystalline TiO₂ photoelectrodes ~20 μm thick (area = 0.25 cm^2) were prepared using a variation of a method reported by Grätzel and co-workers.⁸ Fluorine-doped tin oxide (FTO)-coated glass electrodes

(Nippon Sheet Glass Co., Japan) with a sheet resistance of 8–10 Ω^{-2} and an optical transmission of >80% in the visible range were used. Anatase TiO_2 colloids (particle size \approx 13 nm) were obtained from commercial sources (Ti-nanoxide D/SP, Solaronix). The nanocrystalline TiO_2 thin films of approximately 20 μm thickness were deposited onto the conducting glass by screen-printing. The film was then sintered at 500 °C for 1 h. The film thickness was measured with a Surfcom 1400A surface profiler (Tokyo Seimitsu Co., Ltd.). The electrodes were impregnated with a 50 mM titanium tetrachloride solution and sintered at 500 °C. The dye solutions (2×10^{-4} M) were prepared in 1:1 acetonitrile and *tert*-butyl alcohol solvents. Deoxycholic acid as a co-adsorbent was added to the dye solution at a concentration of 20 mM. The electrodes were immersed in the dye solutions and then kept at 25 °C for 20 h to adsorb the dye onto the TiO_2 surface.

2.3.2. Fabrication of Dye-Sensitized Solar Cells. Photovoltaic measurements were performed in a two-electrode sandwich cell configuration. The dye-deposited TiO_2 film was used as the working electrode and a platinum-coated conducting glass as the counter electrode. The two electrodes were separated by a surlyn spacer (40 μm thick) and sealed up by heating the polymer frame. The electrolyte was composed of 0.6 M dimethylpropyl-imidazolium iodide (DMP1), 0.05 M I_2 , and 0.1 M LiI and TBP 0.5 M in acetonitrile (AN).

2.3.3. Photovoltaic Characterization. The working electrode was illuminated through a conducting glass. The current–voltage characteristics were measured using the previously reported method¹⁰¹ with a solar simulator (AM-1.5, 100 mW/cm², WXS-155S-10; Wacom Denso Co. Japan). Monochromatic incident photon-to-current conversion efficiency (IPCE) for the solar cell, plotted as a function of excitation wavelength, was recorded on a CEP-2000 system (Bunkoh-Keiki Co., Ltd.). Incident photon-to-current conversion efficiency (IPCE) at each incident wavelength was calculated from eq 1,

$$\text{IPCE}(\lambda) = 1240 \left(\frac{I_{sc}}{q\lambda P_0} \right) \quad (1)$$

where I_{sc} is the photocurrent density at short circuit (expressed in units of mA cm⁻²) under monochromatic irradiation, q the elementary charge, λ the wavelength of incident radiation (in nanometers), and P_0 the incident radiative flux (in units of W m⁻²).

3. COMPUTATIONAL DETAILS

Following the computational protocol previously developed by some of us for organic sensitizers,¹⁰² the ground-state equilibrium geometries of the isolated CS1A, CS4A, CSORG1, and CSORG4, as well as that of the isolated carbazole (CZ) unit (Figure 1), were optimized in vacuo, using the B3LYP exchange-correlation (xc) functional¹⁰³ and a 6-31G* basis set,¹⁰⁴ while the UV-vis absorption spectra of the dyes in solution were simulated by time-dependent density functional theory (TDDFT) calculations with the hybrid MPW1K xc functional¹⁰⁵ and a 6-31G* basis set. Solvent (tetrahydrofuran, THF) effects were included by the conductor-like polarizable continuum model (C-PCM),¹⁰⁶ as implemented in GAUSSIAN 09.¹⁰⁷ The dye/semiconductor interface has been modeled by adsorbing the CSORG1, CSORG4, and CS4A in a bidentate coordination mode onto a $(\text{TiO}_2)_{82}$ cluster, obtained by appropriately “cutting” an anatase slab, exposing the majority (101) surface;¹⁰⁸ here, we recall that we recently reported about the structure of the CS1A@ TiO_2 and its dimeric aggregates,⁷⁹ so, for this system, we shall refer to the already published results. For the CS4A and CSORG4, the effect of the CZ unit on the tendency of the dye to form stable aggregates on the semiconductor surface has been also investigated. Following the scheme/methodology developed in ref 47, here, we have modeled two different aggregation patterns selected among the most interacting ones. The nomenclature that we use to label the dimer configurations is illustrated in Figure 2, along with a top view of the anatase TiO_2 (101) surface. Keeping fixed the position of the molecule placed in (0,0), each dimer is labeled by the (x,y) coordinates of the second

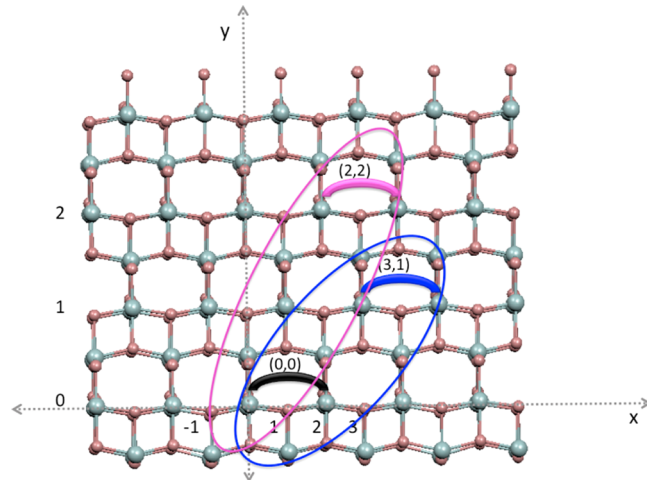


Figure 2. Scheme of the aggregation patterns on the $(\text{TiO}_2)_{82}$ cluster.

molecule. Therefore, the two dimers examined in this study are labeled as (2,2) and (3,1).

The ground-state equilibrium geometries of the CSORG4@(- $\text{TiO}_2)_{82}$, CS4A@($\text{TiO}_2)_{82}$, and those of the corresponding dimeric (2,2) and (3,1) structures have been optimized in the gas phase with the ADF program package,^{109–111} employing the PBE exchange-correlation functional¹¹² with a DZ basis set. The binding energies of the optimized dimeric structures, computed with respect to the non-interacting monomers at the geometry they have in the dimer, were calculated at MP2 level of theory in water solution with a 6-31G* basis set on the deprotonated dimers as cut by the TiO_2 cluster as well as on the same protonated structures at B3LYP-D3^{113,114}/6-31G* in vacuo. The electronic absorption spectra of the protonated dimeric (2,2) and (3,1) CS4A and CSORG4 structures, as well as those of the corresponding isolated molecules, were calculated by TDDFT calculations in THF solution using the MPW1K¹⁰³ and a 6-31G* basis set.

4. RESULTS AND DISCUSSION

4.1. UV-vis Absorption Spectra. In the top panel of Figure 3, the experimental UV-vis absorption spectra in a THF solution of CS1A, CS4A, and the emission spectra of the CZ¹¹⁵ are displayed, whereas, in the bottom panel, we report the absorption spectra (THF solution) of the CSORG1 and CSORG4 sensitizers; the corresponding absorption and emission band maxima are reported in Table 1. Here, we shall leave out the detailed discussion of the optical properties of the CS1A dye, referring the interested reader to our previous work (ref 78).

In the low-energy region, the CZ-free CS1A and CS4A dyes present intense absorption bands, centered at 440 and 465 nm, respectively, being quite well-reproduced by the TDDFT/MPW1K calculations, which locate the lowest-energy vertical transitions at 422 and 451 nm, respectively. The higher-energy bands show maxima at 314 (CS1A) and 356 nm (CS4A), again nicely reproduced by the TDDFT calculations, which, for CS1A, predict two dipole-allowed transitions at 306 and 288 nm, whereas for CS4A, a single excitation at 333 nm. As expected, the introduction of the rhodanine 3-acetic-acid acceptor group yields a moderate red-shift of the absorption spectrum associated to a sizeable increase of the molar absorption coefficient. The absorption spectrum of the CZ ring in apolar solvent (cyclohexane) shows two maxima at 330 and 345 nm,¹¹⁵ which therefore lie within the high-energy absorption band of the PTZ, as highlighted in absorption

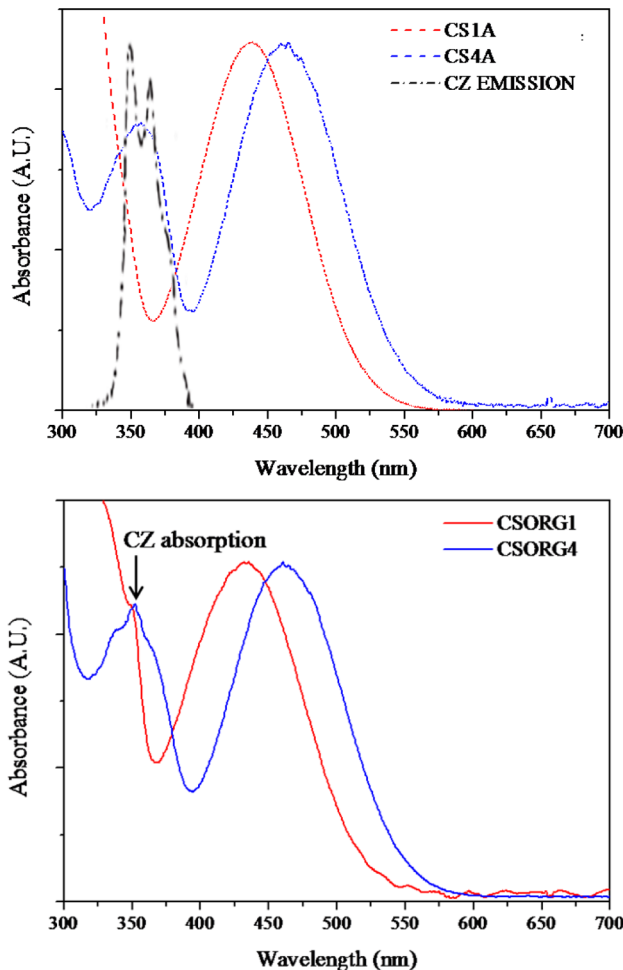


Figure 3. (Top) UV-vis absorption spectra in THF solution of CS1A (dotted red line) and CS4A (dotted blue line) and emission spectrum of CZ from ref 114 (dash-dotted black line). (Bottom) UV-vis absorption spectra in THF solution of CSORG1 (red line) and CSORG4 (blue line).

Table 1. Absorption (λ_{abs}) and Emission Maxima for the Dyes in THF Solution and Adsorbed on TiO_2^a

dye	Experimental	
	λ_{abs} , nm ($\epsilon \times 10^4, \text{M}^{-1} \text{cm}^{-1}$)	λ_{em} , nm
CS1A	440 (1.4), 314 (2.2)	635
CS4A	465 (2.9), 356 (2.2), 299 (2.1)	677
CSORG1	435 (1.9), 350 (1.6), 312 (2.7)	626
CSORG4	460 (3.2), 352 (2.8), 298 (3.3)	673
9-MeCZ ^b	330, 345	350, 365
Calculated		
dye	λ_{abs} , nm/ E_{max} , eV	
CS1A	422/2.94, 306/4.06, 288/4.30	
CS4A	451/2.75, 333/3.72	
CSORG1	421/2.95, 306/4.06, 288/4.30, 260/4.75	
CSORG4	450/2.76, 333/3.72, 260/4.75	

^aThe calculated vertical excitation energies in THF are also reported.

^bData taken from ref 115. Values obtained in cyclohexane.

spectra of the CSORG1 and CSORG4 (top panel of Figure 3), where two peaks imputable to the CZ unit appear at ~ 350 nm. The emission spectrum of CZ,¹¹⁵ reported in the bottom panel of Figure 3, compared with the experimental spectra of the

CS1A and CS4A compounds, shows two peaks at 350 and 365 nm, which therefore favorably match the high-energy absorption of the PTZ, making the FRET accessible for this system. However, we note that the spectral overlap results are sizably larger for the rhodanine-based CS4A dye, increasing, in principle, the probability (Förster radius) of the energy transfer in the CSORG4 sensitizer. The TDDFT-calculated vertical excitation energies reported in Table 1 for CSORG1 and CSORG4 well reproduce the experimental absorption maxima in the low-energy region, where the excitations, involving only the PTZ moiety, have CT character and turn out to be adequately described by the hybrid MPW1K functional (see the isodensity plots of the main molecular orbitals involved in the excitations reported in Figure 4). In the 300–400 nm region, while we predict, with reasonable accuracy, the higher-energy transition of the PTZ (306/288 and 333 nm coincident with those of CS1A and CS4A), the absorption band of the CZ is substantially blue-shifted, being located at 4.25 eV/260 nm. This is not surprising, considering the local $\pi \rightarrow \pi^*$ character of the excitation on the CZ ring (see Figure 4), requiring a lower percentage of Hartree–Fock exchange in the exchange-correlation functional (e.g., B3LYP, PBE0, etc.) to be accurately described.

4.2. Photovoltaic Characterization. Figure 5 displays the IPCE curves for the CSORG1, CSORG4, CS1A, and CS4A dyes.

The CSORG4 dye shows the IPCE onset at 800 nm, whereas the homologous CSORG1 dye onsets at 700 nm, consistent with the red-shift of the absorption spectrum obtained replacing the cyanoacrylic acid anchoring with the rhodanine-3-acetic acid group. However, the IPCE of CSORG1 exceeds 80% in the spectral range of 400–540 nm, unlike CSORG4, which reaches a maximum of 74% at 500 nm. The IPCE spectra of the CZ-free CS1A and CS4A dyes basically show the same shape of the corresponding “complete” dyes but with lowest conversion efficiencies, above all in the case of the rhodanine-based sensitizers, where the introduction of the CZ donor considerably increases the IPCE at both high-energy and low-energy ranges. The higher IPCE in the 300–450 nm range for CSORG1 and CSORG4, compared to CS1A and CS4A, could be possibly attributed to FRET between the CZ donor and the PTZ acceptor. However, the most intriguing difference between CS4A and CSORG4 is the extension from 700 nm up to 800 nm of the IPCE, which is suggestive of the evidently different optical/electronic/structural properties of the sensitized TiO_2 . In Figure 6, the current density–voltage (J – V) curves for the DSSCs are reported, while the related PV data are collected in Table 2.

The increased photocurrent of CSORG4, with respect to CSORG1, is consistent with the red-shifted absorption maximum and the molar extinction coefficients reported in Table 1 and the IPCE curves discussed above. However, we note overall larger V_{oc} values of the cyanoacrylic dyes, compared to the rhodanine-based homologues, possibly indicating accelerated electron recombination processes in the latter. Interestingly, the introduction of the CZ donor slightly lowers the efficiency of the CSORG1 dye, from 6.3% to 5.8%, basically reducing the V_{oc} of ~ 70 mV. As a matter of fact, instead, for the rhodanine-based sensitizers, CSORG4 and CS4A, the presence of the CZ donor notably raises the cell efficiency from 2.5% to 5.6%, yielding a two-fold increase in the photocurrent (from 6.7 to 12.7 mA/cm²), a higher V_{oc} , and also a slightly higher fill factor (FF).

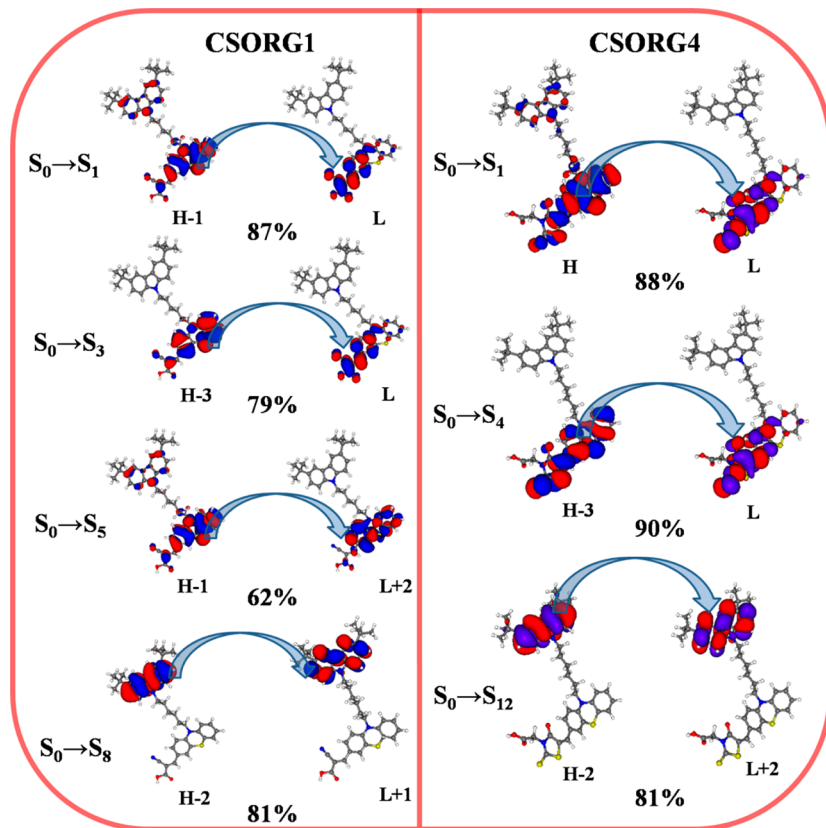


Figure 4. Isodensity plots of relevant molecular orbitals involved in the excited states of CSORG1 and CSORG4; the weight of the predominant excitation for each excited state listed in Table 1 is also reported.

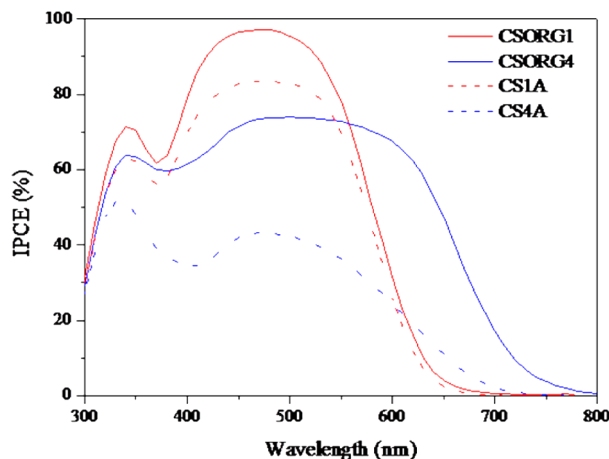


Figure 5. IPCE spectra of CSORG1 (red line), CSORG4 (blue line), CS1A (red dashed line), and CS4A (blue dashed line).

4.3. Modeling the Dye-Sensitized TiO_2 . 4.3.1. Adsorption Geometry and Electronic Properties of the Dye/ TiO_2 Interface. To gain insight into the peculiar effect of the CZ unit, which exceptionally improves the photovoltaic performance of the CSORG4 dye, compared to the PTZ CS4A dye, we investigated the adsorption of a single dye molecule as well as that of two possible dimeric aggregates, on a $(\text{TiO}_2)_{82}$ nanocluster. First, we start by discussing the adsorption geometries of CSORG1, CSORG4, and CS4A on the TiO_2 surface (see Figure 7).

As we have previously shown for other organic dyes bearing the cyanoacrylic and the rhodanine-3-acetic acids, the bidentate

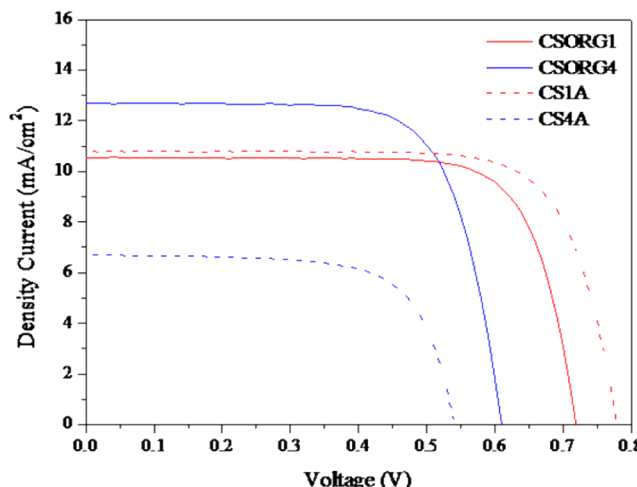


Figure 6. Current density–voltage (J – V) curves of CSORG1 (black line), CSORG4 (red line), CS1A (magenta line), and CS4A (blue line).

Table 2. Photovoltaic Data of the CSORG Series of Dyes

dye	short-circuit current density (J_{sc}), mA/cm ²	short-circuit voltage (V_{oc}), mV	fill factor (FF)	efficiency (η), %
CSORG1	10.5	719	0.76	5.8
CSORG4	12.7	610	0.72	5.6
CS1A	10.8	779	0.75	6.3
CS4A	6.7	541	0.70	2.5

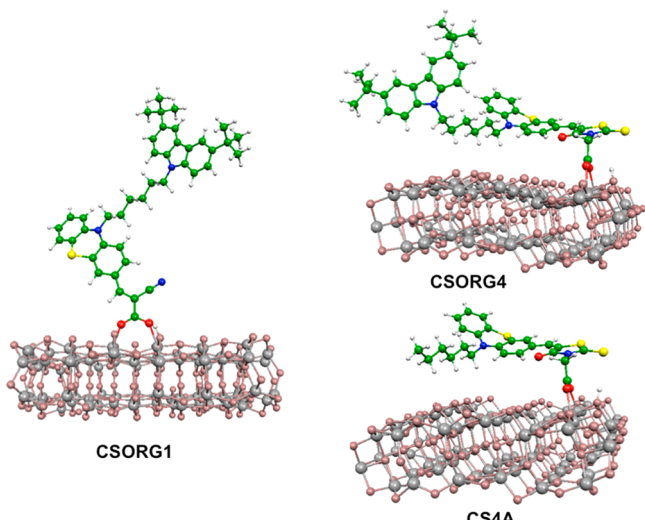


Figure 7. Optimized ground-state geometries of CSORG1@ $(\text{TiO}_2)_{82}$, CSORG4@ $(\text{TiO}_2)_{82}$, and CS4A@ $(\text{TiO}_2)_{82}$.

coordination leads to a molecule standing perpendicular to the semiconductor surface in the former case and to a molecule lying almost flat, with respect to the TiO_2 surface plane, in the latter case.¹¹⁶ We also notice that the presence of CZ in CSORG4 does not change the adsorption geometry, compared to the PTZ CS4A dye. In the upper panel of Figure 8, we compare the projected density of states (PDOS) on the dye's LUMO (upper panel) for the CSORG4@ TiO_2 and

CSORG1@ TiO_2 systems, whereas in the bottom, the corresponding Lorentzian distribution¹¹⁷ of the LUMOs is plotted; note that, here, we do not plot the PDOS of CS4A@ TiO_2 , since it is coincident with that of the CSORG4 dye. By analyzing the PDOSs, an average value of the LUMO of the adsorbed dye ($E_{\text{LUMO}}(\text{ads})$) can be defined as follows:

$$E_{\text{LUMO}}(\text{ads}) = \frac{\sum_i \varepsilon_i p_i}{\sum_i p_i} \quad (2)$$

where ε_i represents the calculated orbital energies and p_i represents the projected DOS (PDOS) contributions on the dyes's LUMO.

This provides us with an estimation of the shift of the LUMO of the isolated dye, as a consequence of the interaction with the TiO_2 states: the larger the electronic interaction between the adsorbate and the substrate, the larger the rate of the electron injection. In fact, according to the Newns–Anderson model,^{118,119} one can estimate the injection rate by simply considering the broadening of the PDOS, relative to the LUMO of the dye, which can be effectively described by a Lorentzian distribution.¹¹⁷ Looking at the plots in Figure 8, one can notice that, as expected, the use of the nonconjugated rhodanine-3-acetic acid group as an anchoring unit in CSORG4 (CS4A) strongly reduces the broadening of the dye's LUMO, with respect to that calculated for the CSORG1 dye. For CSORG4, the value of the adsorbed LUMO is -2.88 eV, coincident with the energy of an orbital having 96% of the electron density localized on the dye, the first CB state is predicted at 3.15 eV and the calculated Lorentzian broadening

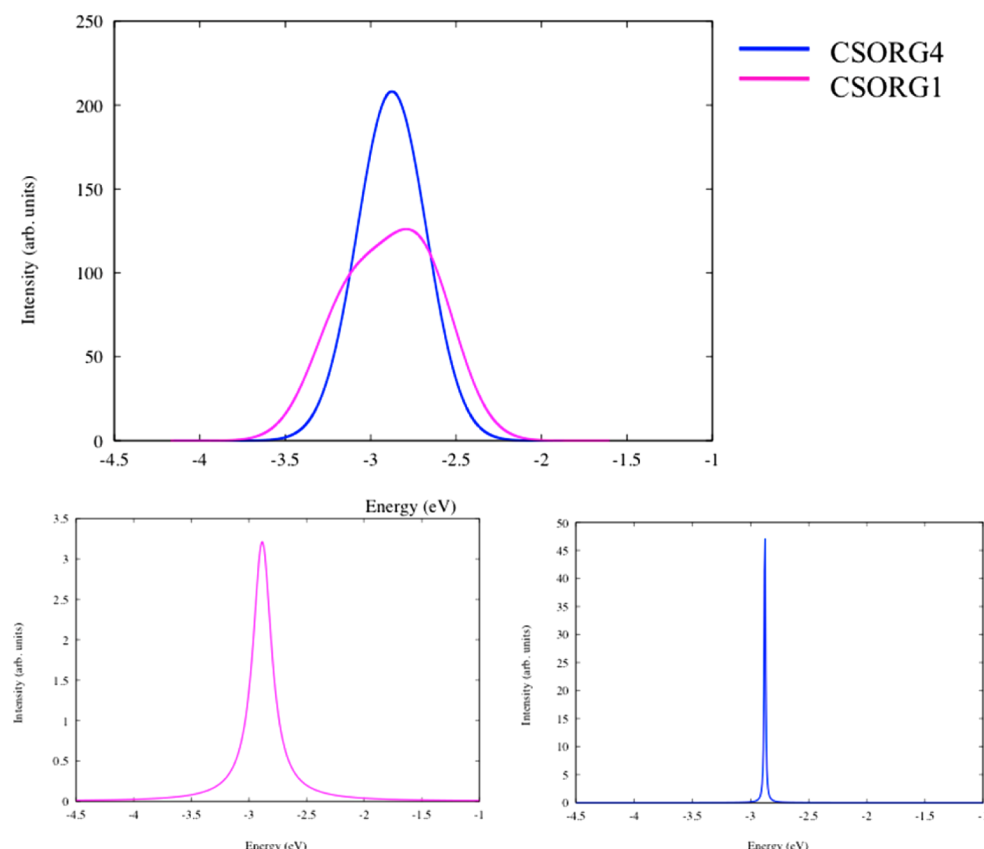


Figure 8. (Top) The dye's LUMO projected density of states (PDOS) plots of CSORG4@ TiO_2 (blue line) and CSORG1@ TiO_2 (magenta line). (Bottom) Lorentzian distributions of the LUMO of CSORG4@ TiO_2 (blue line) and CSORG1@ TiO_2 (magenta line).

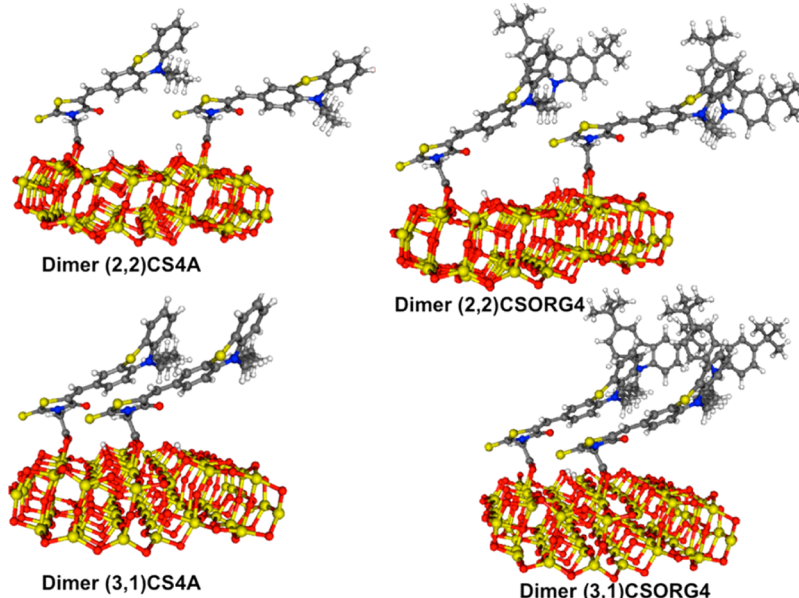


Figure 9. Optimized molecular structures of (2,2) and (3,1) dimers of CS4A@ $(\text{TiO}_2)_{82}$ and CSORG4@ $(\text{TiO}_2)_{82}$.

is 0.012 eV (injection rate of 54 fs); a similar situation is found for the CS4A dye, with the dye's LUMO (ca. 87 %) at -2.87 eV and the lowest TiO_2 empty state at -3.14 eV and a broadening of 0.014 (injection rate of 47 fs). For the cyanoacrylic-based dye, CSORG1, the LUMO is spread over ca. 30 empty states, largely mixed with the TiO_2 conduction band states (see the asymmetric and broadened PDOS in Figure 8) and its average value is -2.88 eV, with the CB edge at -3.17 eV; the resulting Lorentzian broadening is 0.196 eV, corresponding to an injection rate of ca. 3 fs. Hence, our results suggest that such a strong mixing between the dye's LUMO and the TiO_2 empty states might induce an ultrafast direct injection mechanism for the CSORG1 dye, with the electrons that are partially directly excited into the hybrid dye- TiO_2 empty states, whereas for CSORG4 and CS4A, analogous to that discussed for other rhodanine-anchored sensitizers,¹¹⁶ an indirect injection mechanism is supposed to take place.

Moreover, as discussed for analogous threephenylamine-based organic dyes,¹¹⁶ the different adsorption configuration of the rhodanine-anchored sensitizers and their lower electronic coupling with the TiO_2 CB states, compared to the cyanoacrylic-based homologues, might account for the accelerated electron recombination reaction in the former case and thus for their generally lower V_{oc} values.⁵¹

4.3.2. Aggregation. The analysis of the electronic properties of the dye/semiconductor interface discussed above does not provide useful insights for the dramatically different photovoltaic performances of CS4A and CSORG4, since the dyes show the same adsorption mode on the TiO_2 surface and the sensitized- TiO_2 has rather similar electronic structure and energetic (conduction band edge, extent of the TiO_2 -dye's LUMO mixing). Therefore, the considerable improvement in photocurrent, and V_{oc} values obtained passing from CS4A to CSORG4, could be related to peculiar aggregation motifs of the CSORG4 dye, yielding the sizeable red-shift and broadening of the light absorption range. To model the aggregation properties of both CSORG4 and CS4A, here, we investigate the relative stability and the optical response of two close-interacting dimeric arrangements, namely (2,2) and the (3,1) reported in Figure 9 (see the scheme depicted in Figure 2).

The binding energies of the dimeric structures, computed with respect to the non-interacting monomers at the geometry they have in the dimer, are listed in Table 3; the B3LYP-D3

Table 3. Calculated MP2 and B3LYP-D3 Binding Energies for the Dimeric Structures of CS4A and CSORG4

dimer	Binding Energy, kcal/mol	
	B3LYP-D3/prot/vac	MP2/dep/solv
(2,2)-CS4A	3.8	2.5
(3,1)-CS4A	14.2	10.6
(2,2)-CSORG4	3.5	3.1
(3,1)-CSORG4	16.9	13.1

values^{113,114} have been calculated for the protonated dimeric structures in the gas phase, whereas, for the deprotonated dimers, we carried out MP2 calculations in solution.

As is apparent, regardless the level of calculation, the interaction energies do not show significant differences in the aggregation motif of CSORG4, compared to that of the smaller homologue, CS4A: both dyes have a sizeable tendency to form close aggregates, with the (3,1) scheme largely stabilized (more than 10 kcal/mol) with respect to the non-interacting monomers. The CZ units, interacting each other face to face in this static aggregation model, seem to favor the close packing on the oxide surface, slightly increasing the stabilization energy, compared to that of CS4A, with an effect closely resembling that of long alkyl chains. However, we cannot exclude that the thermal motion in the actual devices might induce some steric hindrance and reduce the aggregation strength.

Further insights come from the simulation of the optical absorption spectra of the dimers and from their comparison with those of the isolated monomers optimized on the TiO_2 cluster at the same level of theory. In Figure 10, we compare the simulated absorption spectra of the two investigated dimeric structures and of the isolated dyes, for both CS4A (top panel) and CSORG4 (bottom panel), while the calculated excitation energies and their oscillator strengths are listed in Table 4.

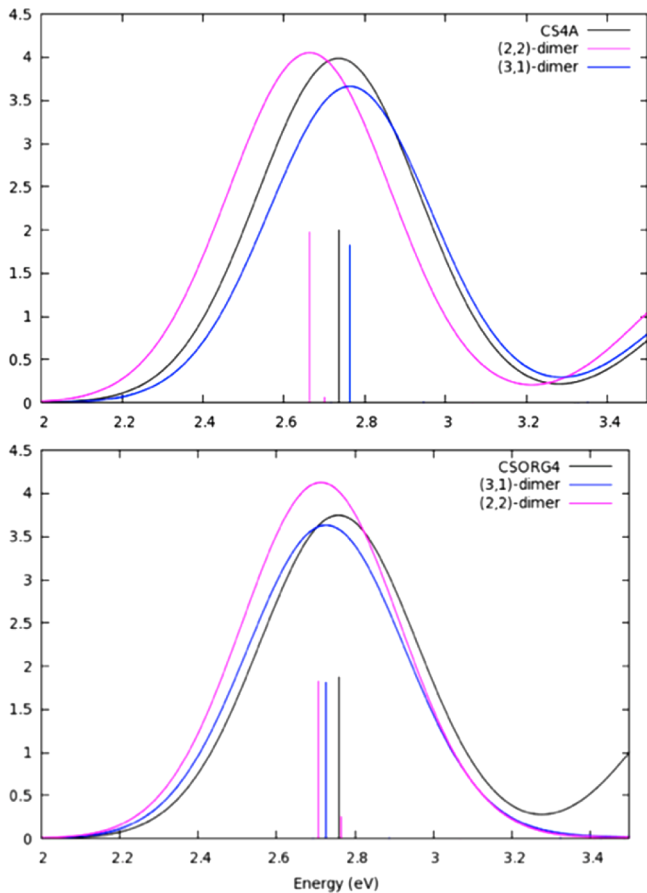


Figure 10. Simulated absorption spectra (MPW1K/6-31G*/ACN) for the (2,2) and (3,1) aggregation schemes, compared to the corresponding monomers of both CS4A (top panel) and CSORG4 (bottom panel).

The (2,2)-type aggregates show, in both cases, an appreciable red-shift, associated to an intensity increment, of the lowest-energy band (magenta lines vs. black lines in Figure 10), which moves from 2.74 eV to 2.66 eV (CS4A) and from 2.76 eV to 2.71 eV (CSORG4). Interestingly, the largely favored (3,1) dimeric structure delivers a differential optical response in the two cases: for the PTZ CS4A dye, a small blue-shift associated to an intensity reduction is calculated, with the band maximum going from 2.74 eV to 2.76 eV, whereas for the CSORG4 dye, a 0.03 red-shift (from 2.76 eV to 2.73 eV) is predicted, with the first transition occurring at 2.69 eV. Therefore, our calculations suggest that both CS4A and CSORG4 tend to give aggregation upon adsorption onto the semiconductor surface. Moreover, the red-shift and intensity increase calculated for the (3,1)

CSORG4, compared to the blue-shift and intensity decrease predicted for the analogous CS4A dimer, could explain the extension of the CSORG4@TiO₂ absorption up to 800 nm, as shown in the IPCE curves in Figure 6. These results give indication of a beneficial effect, already documented in the literature,^{48,120–122} arising from the formation of “benign” surface aggregates, which notably extend the light absorption window. Given the strong tendency to give close packing, one can further speculate that the carbazole units in CSORG4, which closely interact each other in a face-to-face arrangement, provide an effective blocking layer against the I₂/I₃⁻ percolation toward the oxide surface, suppressing electron recombination reactions and thus increasing the open circuit voltage of the cell, compared to that of the CZ-free CS4A dye (see the V_{oc} values in Table 2).

4.3.3. Förster Resonance Energy Transfer (FRET). Following our previous work,⁷³ to model the occurrence of Förster-type intramolecular energy transfer (FRET) between the CZ and the PTZ units, we calculated the dimensionless factor κ^2 , at the optimized geometries of the CSORG1 and CSORG4 dyes adsorbed on the TiO₂ cluster.

We briefly recall that the energy transfer rate is given by

$$k_F = \frac{1}{\tau_0} \left(\frac{R_0^6}{|r_A - r_D|^6} \right) \quad (3)$$

where τ_0 is the lifetime of the donor excited state, R_0 is the Förster radius, and r_D and r_A are the position vectors of the donor and the acceptor respectively. The Förster radius can be obtained from the donor luminescence efficiency (Q_D), the overlap integral of the donor emission spectrum (F_D), and the acceptor absorption spectrum (e_A) and the orientation factor (κ^2):

$$R_0^6 = \frac{9000 \times \ln(10) \kappa^2 Q_D}{128\pi^5 n^4 N_A} \int F_D(\lambda) e_A(\lambda) \lambda^4 d\lambda \quad (4)$$

with N_A being the Avogadro's number and n the refractive index of the medium. The dimensionless orientation factor κ^2 can vary from 0 to 4 and is given by the expression

$$\kappa^2 = (\cos \gamma - 3 \cos \alpha \cos \beta)^2 \quad (5)$$

where the angle α , β , and γ define the relative orientation between the two interacting dipole moments.⁷⁷ As discussed above, the larger spectral overlap between the CZ emission and the CS4A absorption spectra, compared to CS1A in Figure 3, implies, with other factors being equal, a more favorable FRET in the case of the CSORG4 dye, compared to CSORG1. Furthermore, the different adsorption geometries, induced by the two different anchoring groups in CSORG1 and CSORG4

Table 4. Calculated (MPW1K/6-31G*/ACN) Lowest Singlet Excitation Energies (E_{exc}), Oscillator Strengths (f), and Band Maxima (E_{max}) for the (2,2) and (3,1) Dimeric Arrangements and of the Corresponding Isolated Monomer for Both CS4A and CSORG4

dye	Monomer			(2,2) Dimer			(3,1) Dimer		
	E_{max} eV	E_{exc} eV	f	E_{max} eV	E_{exc} eV	f	E_{max} eV	E_{exc} eV	f
CSORG4	2.76	2.76	0.939	2.71	2.71	1.823	2.73	2.69	0.006
				2.76	2.76	0.255		2.72	1.807
CS4A	2.74	2.74	1.000	2.66	2.66	1.970	2.76	2.72	0.007
				2.70	2.70	0.063		2.76	1.821

dyes (see Figure 7), yield different relative orientations of the donor (CZ) and acceptor (PTZ) moieties and possibly different donor–acceptor distances. Actually, we calculated markedly different κ^2 values: 1.81 and 3.17 for CSORG1 and CSORG4, respectively, with donor–acceptor distances (distances between centers of nuclear charges) of 11.75 and 10.88 Å, respectively. It is worthwhile to highlight here that (i) the calculated parameters refer to a “static” model where the relative donor/acceptor orientation is kept fixed and (ii) the introduction of dynamical effects might induce temporal variations of the calculated distances and κ^2 values. However, one can speculate that the interaction with the semiconductor surface and the close molecular packing, attested by the strong dimerization energies discussed above, should limit the random rotation of the CZ antenna, as well as important geometrical rearrangements of the system, making us confident that this “static” picture provides a reliable “average” model of the FRET process.

In summary, the present results confirm the possible occurrence of FRET from CZ to PTZ in both molecules, although with a possibly larger Förster radius (higher energy transfer rate) in the rhodanine-based dye, possibly accounting for the increase in the light absorption and the increase in the generated photocurrent in the 350–400 nm window.

5. CONCLUSIONS

We have reported the synthesis, photovoltaic characterization, and computational modeling of two new organic phenothiazine dyes, obtained by linking, via a C₆H₁₂ alkyl chain, a donor carbazole moiety to the phenothiazine core, which is anchored to the TiO₂ surface either through a cyanoacrylic acid (CSORG1) or a rhodanine-3-acetic acid (CSORG4). The introduction of the carbazole donor was shown to remarkably enhance the photovoltaic performances of the rhodanine-based dye (CSORG4), compared to the corresponding simple PTZ dye (CS4A), with more than a two-fold increase in the overall efficiencies. On the other side, the carbazole did not bring beneficial effects in the case of the cyanoacrylic-based sensitizers, even yielding a slightly lower efficiency for CSORG1, compared to CS1A. In order to provide an explanation of the PV data and understand the role of the carbazole unit, we modeled the stand-alone molecules in solution as well as the dye-sensitized TiO₂, investigating the structural, electronic, and optical properties of the dye/semiconductor interface, the dye aggregation, and the possible occurrence of beneficial intramolecular energy transfer (FRET) from the carbazole to the phenothiazine. The computational study suggests that both CS4A and CSORG4 dyes tend to give aggregation upon adsorption onto semiconductor surface, contrary to that previously found for the cyanoacrylic-based CS1A dye. Moreover, the clear red-shift and intensity increase calculated for the most stable CSORG4 dimer, compared to the blue-shift and intensity decrease predicted for the analogous CS4A dimer, could provide an explanation of the extension of the CSORG4@TiO₂ absorption up to 800 nm. We also speculate that the carbazole units in the CSORG4, which tend to closely interact each other in a face-to-face arrangement, provide an effective blocking layer for the percolation of the redox species toward the oxide surface. Moreover, the carbazole core is possibly responsible of a intramolecular fluorescence resonance energy transfer, which based on the absorption and emission spectra overlap and on the calculated values of the

orientational κ^2 factor, turns out to be largely favored in the rhodanine-3-acetic acid-based CSORG4 dye.

Our study demonstrates that a proper molecular design, by accurate selection of donor, acceptor, and anchoring groups, combined with a high-level computational modeling of the structural and optical/electronic properties of the dye-sensitized interface, may provide remarkable advances toward the efficiency boost direction.

■ AUTHOR INFORMATION

Corresponding Author

*E-mail:chiara@thch.unipg.it (M.P.), filippo@thch.unipg.it (F.D.A.), chandra@iict.res.in (M.C.).

Notes

The authors declare no competing financial interest.

■ ACKNOWLEDGMENTS

The authors acknowledge the financial support from the joint FP7-ENERGY 2010 (Contract No. 261920) and DST, New Delhi, project “Efficient Solar Cells based on Organic and Hybrid Technology (ESCORT)”.

■ REFERENCES

- (1) Grätzel, M. *Acc. Chem. Res.* **2009**, *42*, 1788–1798.
- (2) Nazeeruddin, M. K.; De Angelis, F.; Fantacci, S.; Selloni, A.; Viscardi, G.; Liska, P.; Ito, S.; Takeru, B.; Grätzel, M. *J. Am. Chem. Soc.* **2005**, *127*, 16835–16847.
- (3) O'Regan, B.; Grätzel, M. *Nature* **1991**, *353*, 737–740.
- (4) Nazeeruddin, M. K.; Kay, A.; Rodicio, I.; Humphry-Baker, R.; Mueller, E.; Liska, P.; Vlachopoulos, N.; Grätzel, M. *J. Am. Chem. Soc.* **1993**, *115*, 6382–6390.
- (5) Boschloo, G.; Hagfeldt, A. *Acc. Chem. Res.* **2009**, *42*, 1819–1826.
- (6) K. Nazeeruddin, M.; Péchy, P.; Grätzel, M. *Chem. Commun.* **1997**, *, 1705–1706.*
- (7) Nazeeruddin, M. K.; Zakeeruddin, S. M.; Humphry-Baker, R.; Jirousek, M.; Liska, P.; Vlachopoulos, N.; Shklover, V.; Fischer, C.-H.; Grätzel, M. *Inorg. Chem.* **1999**, *38*, 6298–6305.
- (8) Nazeeruddin, M. K.; Péchy, P.; Renouard, T.; Zakeeruddin, S. M.; Humphry-Baker, R.; Comte, P.; Liska, P.; Cevey, L.; Costa, E.; Shklover, V.; Spiccia, L.; Deacon, G. B.; Bignozzi, C. A.; Grätzel, M. *J. Am. Chem. Soc.* **2001**, *123*, 1613–1624.
- (9) Mishra, A.; Fischer, M. K. R.; Bäuerle, P. *Angew. Chem., Int. Ed.* **2009**, *48*, 2474–2499.
- (10) Chandrasekham, M.; Chiranjeevi, B.; Gupta, K. S. V.; Singh, S. P.; Islam, A.; Han, L.; Kantam, M. L. *J. Nanosci. Nanotechnol.* **2012**, *12*, 4489–4494.
- (11) Ito, S.; Miura, H.; Uchida, S.; Takata, M.; Sumioka, K.; Liska, P.; Comte, P.; Péchy, P.; Grätzel, M. *Chem. Commun.* **2008**, *, 5194–5196.*
- (12) Zeng, W.; Cao, Y.; Bai, Y.; Wang, Y.; Shi, Y.; Zhang, M.; Wang, F.; Pan, C.; Wang, P. *Chem. Mater.* **2010**, *22*, 1915–1925.
- (13) Hara, K.; Sato, T.; Katoh, R.; Furube, A.; Yoshihara, T.; Murai, M.; Kurashige, M.; Ito, S.; Shinpo, A.; Suga, S. *Adv. Funct. Mater.* **2005**, *15*, 246–252.
- (14) Hara, K.; Kurashige, M.; Ito, S.; Shinpo, A.; Suga, S.; Sayama, K.; Arakawa, H. *Chem. Commun.* **2003**, *, 252–253.*
- (15) Hara, K.; Kurashige, M.; Dan-oh, Y.; Kasada, C.; Shinpo, A.; Suga, S.; Sayama, K.; Arakawa, K. *New. J. Chem.* **2003**, *27*, 783–785.
- (16) Hara, K.; Sayama, K.; Ohga, Y.; Shinpo, A.; Suga, S.; Arakawa, H. *Chem. Commun.* **2001**, *, 569–570.*
- (17) Hara, K.; Tachibana, Y.; Ohga, Y.; Shinpo, A.; Suga, S.; Sayama, K.; Sugihara, H.; Arakawa, H. *Sol. Energy Mater. Sol. Cells* **2003**, *77*, 89–103.
- (18) Hara, K.; Wang, Z.-S.; Sato, T.; Furube, A.; Katoh, R.; Sugihara, H.; Dan-oh, Y.; Kasada, C.; Shinpo, A.; Suga, S. *J. Phys. Chem. B* **2005**, *15476–15482.*

- (19) Hara, K.; Miyamoto, K.; Abe, Y.; Yanagida, M. *J. Phys. Chem. B* **2005**, *109*, 23776–23778.
- (20) Hara, K.; Sato, T.; Katoh, R.; Furube, A.; Ohga, Y.; Shinpo, A.; Suga, S.; Sayama, K.; Sugihara, H.; Arakawa, H. *J. Phys. Chem. B* **2003**, *107*, 597–606.
- (21) Wang, Z.-S.; Cui, Y.; Dan-oh, Y.; Kasada, C.; Shinpo, A.; Hara, K. *J. Phys. Chem. C* **2007**, *111*, 7224–7230.
- (22) Chen, R.; Yang, X.; Tian, H.; Sun, L. *J. Photochem. Photobiol. A: Chem.* **2007**, *189*, 295–300.
- (23) Chen, R.; Yang, X.; Tian, H.; Wang, X.; Hagfeldt, A.; Sun, L. *Chem. Mater.* **2007**, *19*, 4007–4015.
- (24) Campbell, W. M.; Jolley, K. W.; Wagner, P.; Wagner, K.; Walsh, P. J.; Gordon, K. C.; Schmidt-Mende, L.; Nazeeruddin, M. K.; Wang, Q.; Grätzel, M.; Officer, D. L. *J. Phys. Chem. C* **2007**, *111*, 11760–11762.
- (25) Wang, Z.-S.; Cui, Y.; Dan-oh, Y.; Kasada, C.; Shinpo, A.; Hara, K. *J. Phys. Chem. C* **2008**, *112*, 17011–17017.
- (26) Thomas, K. R. J.; Lin, J. T.; Hsu, Y.-C.; Ho, K.-C. *Chem. Commun.* **2005**, , 4098–4100.
- (27) Hwang, S.; Lee, J. H.; Park, C.; Lee, H.; Kim, C.; Park, C.; Lee, M.-H.; Lee, W.; Park, J.; Kim, K.; Park, N.-G.; Kim, C. *Chem. Commun.* **2007**, , 4887–4889.
- (28) Xu, W.; Peng, B.; Chen, J.; Liang, M.; Cai, F. *J. Phys. Chem. C* **2008**, *112*, 874–880.
- (29) Liu, W. H.; Wu, I. C.; Lai, C. H.; Lai, C. H.; Chou, P. T.; Li, Y. T.; Chen, C. L.; Hsu, Y. Y.; Chi, Y. *Chem. Commun.* **2008**, 5152–5154.
- (30) Hagberg, D. P.; Marinado, T.; Karlsson, K. M.; Nonomura, K.; Qin, P.; Boschloo, G.; Brinck, T.; Hagfeldt, A.; Sun, L. *J. Org. Chem.* **2007**, *72*, 9550–9556.
- (31) Tian, H.; Yang, X.; Chen, R.; Pan, Y.; Li, L.; Hagfeldt, A.; Sun, L. *Chem. Commun.* **2007**, *0*, 3741–3743.
- (32) Tan, S.; Zhai, J.; Fang, H.; Jiu, T.; Ge, J.; Li, Y.; Jiang, L.; Zhu, D. *Chem.—Eur. J.* **2005**, *11*, 6272–6276.
- (33) Tanaka, K.; Takimiya, K.; Otsubo, T.; Kawabuchi, K.; Kajihara, S.; Harima, Y. *Chem. Lett.* **2006**, *35*, 592–593.
- (34) Yum, J.-H.; Walter, P.; Huber, S.; Rentsch, D.; Geiger, T.; Nüesch, F.; De Angelis, F.; Grätzel, M.; Nazeeruddin, M. K. *J. Am. Chem. Soc.* **2007**, *129*, 10320–10321.
- (35) Schmidt-Mende, L.; Bach, U.; Humphry-Baker, R.; Horiuchi, T.; Miura, H.; Ito, S.; Uchida, S.; Grätzel, M. *Adv. Mater.* **2005**, *17*, 813–815.
- (36) Horiuchi, T.; Miura, H.; Sumioka, K.; Uchida, S. *J. Am. Chem. Soc.* **2004**, *126*, 12218–12219.
- (37) Horiuchi, T.; Miura, H.; Uchida, S. *Chem. Commun.* **2003**, *0*, 3036–3037.
- (38) Mosconi, E.; Yum, J.-H.; Kessler, F.; Gómez García, C. J.; Zuccaccia, C.; Cinti, A.; Nazeeruddin, M. K.; Grätzel, M.; De Angelis, F. *J. Am. Chem. Soc.* **2012**, *134*, 19438–19453.
- (39) Yella, A.; Lee, H.-W.; Tsao, H. N.; Yi, C.; Chandiran, A. K.; Nazeeruddin, M. K.; Diau, E. W.-G.; Yeh, C.-Y.; Zakeeruddin, S. M.; Grätzel, M. *Science* **2011**, *334*, 629–634.
- (40) Daeneke, T.; Kwon, T.-H.; Holmes, A. B.; Duffy, N. W.; Bach, U.; Spiccia, L. *Nat. Chem.* **2011**, *3*, 211–215.
- (41) Feldt, S. M.; Gibson, E. A.; Gabrielsson, E.; Sun, L.; Boschloo, G.; Hagfeldt, A. *J. Am. Chem. Soc.* **2010**, *132*, 16714–16724.
- (42) Han, L.; Islam, A.; Chen, H.; Malapaka, C.; Chiranjeevi, B.; Zhang, S.; Yang, X.; Yanagida, M. *Energy Environ. Sci.* **2012**, *5*, 6057–6060.
- (43) Hara, K.; Miyamoto, K.; Abe, Y.; Yanagida, M. *J. Phys. Chem. B* **2005**, *109*, 23776–23778.
- (44) Burfeindt, B.; Hannappel, T.; Storck, W.; Willig, F. *J. Phys. Chem.* **1996**, *100*, 16463–16465.
- (45) Liu, D.; Fessenden, R. W.; Hug, G. L.; Kamat, P. V. *J. Phys. Chem. B* **1997**, *101*, 2583–2590.
- (46) Miyashita, M.; Sunahara, K.; Nishikawa, T.; Uemura, Y.; Koumura, N.; Hara, K.; Mori, A.; Abe, T.; Suzuki, E.; Mori, S. *J. Am. Chem. Soc.* **2008**, *130*, 17874–17881.
- (47) Pastore, M.; Angelis, F. D. *ACS Nano* **2009**, *4*, 556–562.
- (48) Sayama, K.; Tsukagoshi, S.; Hara, K.; Ohga, Y.; Shinpou, A.; Abe, Y.; Suga, S.; Arakawa, H. *J. Phys. Chem. B* **2002**, *106*, 1363–1371.
- (49) Tatay, S.; Haque, S. A.; O'Regan, B.; Durrant, J. R.; Verhees, W. J. H.; Kroon, J. M.; Vidal-Ferran, A.; Gavina, P.; Palomares, E. *J. Mater. Chem.* **2007**, *17*, 3037–3044.
- (50) Tian, H.; Yang, X.; Chen, R.; Zhang, R.; Hagfeldt, A.; Sun, L. *J. Phys. Chem. C* **2008**, *112*, 11023–11033.
- (51) Wiberg, J.; Marinado, T.; Hagberg, D. P.; Sun, L.; Hagfeldt, A.; Albinsson, B. *J. Phys. Chem. C* **2009**, *113*, 3881–3886.
- (52) Pastore, M.; Mosconi, E.; De Angelis, F. *J. Phys. Chem. C* **2012**, *116*, 5965–5973.
- (53) Kay, A.; Grätzel, M. *J. Phys. Chem.* **1993**, *97*, 6272–6277.
- (54) Zhang, Z.; Zakeeruddin, S. M.; O'Regan, B. C.; Humphry-Baker, R.; Grätzel, M. *J. Phys. Chem. B* **2005**, *109*, 21818–21824.
- (55) Zhang, Z.; Evans, N.; Zakeeruddin, S. M.; Humphry-Baker, R.; Grätzel, M. *J. Phys. Chem. C* **2006**, *111*, 398–403.
- (56) Wang, P.; Zakeeruddin, S. M.; Humphry-Baker, R.; Moser, J. E.; Grätzel, M. *Adv. Mater.* **2003**, *15*, 2101–2104.
- (57) Wang, P.; Zakeeruddin, S. M.; Comte, P.; Charvet, R.; Humphry-Baker, R.; Grätzel, M. *J. Phys. Chem. B* **2003**, *107*, 14336–14341.
- (58) Wang, M.; Li, X.; Lin, H.; Pechy, P.; Zakeeruddin, S. M.; Grätzel, M. *Dalton Trans.* **2009**, *0*, 10015–10020.
- (59) O'Regan, B. C.; Walley, K.; Juozapavicius, M.; Anderson, A.; Matar, F.; Ghaddar, T.; Zakeeruddin, S. M.; Klein, C. d.; Durrant, J. R. *J. Am. Chem. Soc.* **2009**, *131*, 3541–3548.
- (60) O'Regan, B. C.; López-Duarte, I.; Martínez-Díaz, M. V.; Forneli, A.; Albero, J.; Morandeira, A.; Palomares, E.; Torres, T.; Durrant, J. R. *J. Am. Chem. Soc.* **2008**, *130*, 2906–2907.
- (61) Liang, Y.; Peng, B.; Chen, J. *J. Phys. Chem. C* **2010**, *114*, 10992–10998.
- (62) Kim, J.-J.; Lim, K.; Choi, H.; Fan, S.; Kang, M.-S.; Gao, G.; Kang, H. S.; Ko, J. *Inorg. Chem.* **2010**, *49*, 8351–8357.
- (63) Wang, Z.-S.; Koumura, N.; Cui, Y.; Takahashi, M.; Sekiguchi, H.; Mori, A.; Kubo, T.; Furube, A.; Hara, K. *Chem. Mater.* **2008**, *20*, 3993–4003.
- (64) Planells, M.; Pelleja, L.; Clifford, J. N.; Pastore, M.; De Angelis, F.; Lopez, N.; Marder, S. R.; Palomares, E. *Energy Environ. Sci.* **2011**, *4*, 1820–1829.
- (65) Nishida, J.-i.; Masuko, T.; Cui, Y.; Hara, K.; Shibuya, H.; Ihara, M.; Hosoyama, T.; Goto, R.; Mori, S.; Yamashita, Y. *J. Phys. Chem. C* **2010**, *114*, 17920–17925.
- (66) Koumura, N.; Wang, Z.-S.; Mori, S.; Miyashita, M.; Suzuki, E.; Hara, K. *J. Am. Chem. Soc.* **2006**, *128*, 14256–14257.
- (67) Barea, E. M.; Zafer, C.; Gultekin, B.; Aydin, B.; Koyuncu, S.; Icli, S.; Santiago, F. F.; Bisquert, J. *J. Phys. Chem. C* **2010**, *114*, 19840–19848.
- (68) Bai, Y.; Zhang, J.; Zhou, D.; Wang, Y.; Zhang, M.; Wang, P. *J. Am. Chem. Soc.* **2011**, *133*, 11442–11445.
- (69) Förster, T. *Discuss. Faraday Soc.* **1959**, *27*, 7–17.
- (70) Odobel, F.; Pellegrin, Y.; Warnan, J. *Energy Environ. Sci.* **2013**, *6*, 2041–2052.
- (71) Hardin, B. E.; Sellinger, A.; Moehl, T.; Humphry-Baker, R.; Moser, J.-E.; Wang, P.; Zakeeruddin, S. M.; Grätzel, M.; McGehee, M. *D. J. Am. Chem. Soc.* **2011**, *133*, 10662–10667.
- (72) Siegers, C.; Würfel, U.; Zistler, M.; Gores, H.; Hohl-Ebinger, J.; Hinsch, A.; Haag, R. *ChemPhysChem* **2008**, *9*, 793–798.
- (73) Pastore, M.; Angelis, F. D. *J. Phys. Chem. Lett.* **2012**, *3*, 2146–2153.
- (74) Warnan, J.; Pellegrin, Y.; Blart, E.; Odobel, F. *Chem. Commun.* **2012**, *48*, 675–677.
- (75) Cheon, J. H.; Kim, S. A.; Ahn, K.-S.; Kang, M.-S.; Kim, J. H. *Electrochimica Acta* **2012**, *68*, 240–245.
- (76) Hoke, E. T.; Hardin, B. E.; McGehee, M. D. *Opt. Express* **2010**, *18*, 3893–3904.
- (77) Mårtensson, J. *Chem. Phys. Lett.* **1994**, *229*, 449–456.
- (78) Pastore, M.; De Angelis, F. *J. Phys. Chem. Lett.* **2013**, *4*, 956–974.

- (79) Agrawal, S.; Pastore, M.; Marotta, G.; Reddy, M. A.; Chandrasekharan, M.; De Angelis, F. *J. Phys. Chem. C* **2013**, *117*, 9613–9622.
- (80) Tian, H.; Yang, X.; Chen, R.; Pan, Y.; Li, L.; Hagfeldt, A.; Sun, L. *Chem. Commun.* **2007**, , 3741–3743.
- (81) Kim, S. H.; Kim, H. W.; Sakong, C.; Namgoong, J.; Park, S. W.; Ko, M. J.; Lee, C. H.; Lee, W. I.; Kim, J. P. *Org. Lett.* **2011**, *13*, 5784–5787.
- (82) Marszalek, M.; Nagane, S.; Ichake, A.; Humphry-Baker, R.; Paul, V.; Zakeeruddin, S. M.; Grätzel, M. *J. Mater. Chem.* **2012**, *22*, 889–894.
- (83) Meyer, T.; Ogermann, D.; Pankrath, A.; Kleinermanns, K.; Müller, T. J. *J. Org. Chem.* **2012**, *77*, 3704–3715.
- (84) Park, S. S.; Won, Y. S.; Choi, Y. C.; Kim, J. H. *Energy Fuels* **2009**, *23*, 3732–3736.
- (85) Tian, H.; Yang, X.; Chen, R.; Hagfeldt, A.; Sun, L. *Energy Environ. Sci.* **2009**, *2*, 674–677.
- (86) Tsao, M.-H.; Wu, T.-Y.; Wang, H.-P.; Sun, I. W.; Su, S.-G.; Lin, Y.-C.; Chang, C.-W. *Mater. Lett.* **2011**, *65*, 583–586.
- (87) Wan, Z.; Jia, C.; Duan, Y.; Zhou, L.; Lin, Y.; Shi, Y. *J. Mater. Chem.* **2012**, *22*, 25140–25147.
- (88) Wu, W.; Yang, J.; Hua, J.; Tang, J.; Zhang, L.; Long, Y.; Tian, H. *J. Mater. Chem.* **2010**, *20*, 1772–1779.
- (89) Yang, C.-J.; Chang, Y. J.; Watanabe, M.; Hon, Y.-S.; Chow, T. J. *J. Mater. Chem.* **2012**, *22*, 4040–4049.
- (90) Yin, J.-F.; Chen, J.-G.; Lin, J.-T. s.; Bhattacharya, D.; Hsu, Y.-C.; Lin, H.-C.; Ho, K.-C.; Lu, K.-L. *J. Mater. Chem.* **2012**, *22*, 130–139.
- (91) Cao, D.; Peng, J.; Hong, Y.; Fang, X.; Wang, L.; Meier, H. *Org. Lett.* **2011**, *13*, 1610–1613.
- (92) Qiu, X.; Lu, R.; Zhou, H.; Zhang, X.; Xu, T.; Liu, X.; Zhao, Y. *Tetrahedron Lett.* **2008**, *49*, 7446–7449.
- (93) Teng, C.; Yang, X.; Yuan, C.; Li, C.; Chen, R.; Tian, H.; Li, S.; Hagfeldt, A.; Sun, L. *Org. Lett.* **2009**, *11*, 5542–5545.
- (94) Tang, J.; Hua, J.; Wu, W.; Li, J.; Jin, Z.; Long, Y.; Tian, H. *Energy Environ. Sci.* **2010**, *3*, 1736–1745.
- (95) Zhang, X.-H.; Wang, Z.-S.; Cui, Y.; Koumura, N.; Furube, A.; Hara, K. *J. Phys. Chem. C* **2009**, *113*, 13409–13415.
- (96) Chen, C.-Y.; Pootrakulchote, N.; Wu, S.-J.; Wang, M.; Li, J.-Y.; Tsai, J.-H.; Wu, C.-G.; Zakeeruddin, S. M.; Grätzel, M. *J. Phys. Chem. C* **2009**, *113*, 20752–20757.
- (97) Chen, C.-Y.; Chen, J.-G.; Wu, S.-J.; Li, J.-Y.; Wu, C.-G.; Ho, K. C. *Angew. Chem., Int. Ed.* **2008**, *47*, 7342–7345.
- (98) Chandrasekharan, M.; Rajkumar, G.; Suresh, T.; Rao, C. S.; Reddy, P. Y.; Yum, J.-H.; Nazeeruddin, M. K.; Grätzel, M. *Adv. OptoElectronics* **2011**, *2011*, 10.
- (99) Siegers, C.; Hohl-Ebinger, J.; Zimmermann, B.; Würfel, U.; Mühlaupt, R.; Hinsch, A.; Haag, R. *ChemPhysChem* **2007**, *8*, 1548–1556.
- (100) Eichberger, R.; Strothkämper, C.; Thomas, I.; Hannappel, T.; Schwarzburg, K.; Fasting, C.; Bartelt, A.; Schütz, R. *J. Photon. Energy* **2012**, *2*, 021003-1–.
- (101) Koide, N.; Han, L. *Rev. Sci. Instrum.* **2004**, *75*, 2828–2831.
- (102) Pastore, M.; Mosconi, E.; De Angelis, F.; Grätzel, M. *J. Phys. Chem. C* **2010**, *114*, 7205–7212.
- (103) Becke, A. D. *J. Chem. Phys.* **1993**, *98*, 1372–1377.
- (104) Binkley, J. S.; Pople, J. A.; Hehre, W. J. *J. Am. Chem. Soc.* **1980**, *102*, 939–947.
- (105) Lynch, B. J.; Fast, P. L.; Harris, M.; Truhlar, D. G. *J. Phys. Chem. A* **2000**, *104*, 4811–4815.
- (106) Cossi, M.; Rega, N.; Scalmani, G.; Barone, V. *J. Comput. Chem.* **2003**, *24*, 669–681.
- (107) Frisch, M. J.; Trucks, G. W.; Schlegel, H. B.; Scuseria, G. E.; Robb, M. A.; Cheeseman, J. R.; Scalmani, G.; Barone, V.; Mennucci, B.; Petersson, G. A.; et al. *Gaussian 09*, Gaussian, Wallingford, CT, 2009.
- (108) Vittadini, A.; Selloni, A.; Rotzinger, F. P.; Grätzel, M. *Phys. Rev. Lett.* **1998**, *81*, 2954–2957.
- (109) Fonseca Guerra, C.; Snijders, J. G.; ten Velde, G.; Baerends, E. J. *Theor. Chem. Acc.* **1998**, *99*, 391–403.
- (110) ten Velde, G.; Bickelhaupt, F. M.; Baerends, E. J.; Fonseca Guerra, C.; van Gisbergen, S. J. A.; Snijders, J. G.; Ziegler, T. *J. Comput. Chem.* **2001**, *22*, 931–967.
- (111) Baerends, E. J.; Ziegler, T.; Autschbach, J.; Bashford, D.; Bérces, A.; Bickelhaupt, F. M.; Bo, C.; Boerrigter, P. M.; Cavallo, L.; et al. *ADF2012, SCM, Theoretical Chemistry*; Vrije Universiteit: Amsterdam, The Netherlands, 2012; available via the Internet at <http://www.scm.com>.
- (112) Perdew, J. P.; Burke, K.; Ernzerhof, M. *Phys. Rev. Lett.* **1996**, *77*, 3865–3868.
- (113) Grimme, S.; Antony, J.; Ehrlich, S.; Krieg, H. *J. Chem. Phys.* **2010**, *132*, 154104–154123.
- (114) Grimme, S.; Ehrlich, S.; Goerigk, L. *J. Comput. Chem.* **2011**, *32*, 1456–1465.
- (115) Romero-Ale, E. E.; Olives, A. I.; Martin, M. A.; del Castillo, B.; López-Alvarado, P.; Menéndez, J. C. *Luminescence* **2005**, *20*, 162–169.
- (116) Pastore, M.; De Angelis, F. *Phys. Chem. Chem. Phys.* **2012**, *14*, 920–928.
- (117) Cohen-Tannoudji, C.; Diu, B.; Laloë, F. *Quantum Mechanics*, Vol. 2; Wiley: New York, 1977.
- (118) Muscat, J. P.; Newns, D. M. *Progr. Surf. Sci.* **1978**, *9*, 1–43.
- (119) Persson, P.; Lundqvist, M. J.; Ernstorfer, R.; Goddard, W. A.; Willig, F. *J. Chem. Theory Comput.* **2006**, *2*, 441–451.
- (120) Khazraji, A. C.; Hotchandani, S.; Das, S.; Kamat, P. V. *J. Phys. Chem. B* **1999**, *103*, 4693–4700.
- (121) Kawasaki, M.; Aoyama, S. *Chem. Commun.* **2004**, , 988–989.
- (122) Ehret, A.; Stuhl, L.; Spitler, M. T. *J. Phys. Chem. B* **2001**, *105*, 9960–9965.